![USGS logo — science for a changing world]

Bedrock Mapping and Seismic Hazard Assessment at Gold Basin Landslide, Washington

By Lydia M. Staisch

U.S. Department of the Interior
RYAN K. ZINKE, Secretary

U.S. Geological Survey
James F. Reilly II, Director

U.S. Geological Survey, Reston, Virginia: 2018

Contents

Figures

Tables

Bedrock Mapping and Seismic Hazard Assessment at Gold Basin Landslide, Washington

By Lydia M. Staisch

Background

The Gold Basin landslide is located along the South Fork Stillaguamish River, within the Mount Baker-Snoqualmie National Forest in western Washington State (fig. 1). Recent concerns related to slope stability after the 2014 State Route 530 Landslide near Oso, Washington, forced the closure of the U.S. Forest Service Gold Basin Campground in May of 2014. In addition to safety concerns for National Forest visitors, the landslide-derived sediment pulses shed into the South Fork Stillaguamish River may harm migrant salmon spawning grounds (Shannon & Wilson Engineers, 1954; Benda and Collins, 1992), an important resource for the Stillaguamish Tribe of Indians and for public anglers.

The Gold Basin landslide is composed of three active lobes and has an approximate footprint of 566,560 m^2 (Anchor QEA LLC, 2012). Each lobe consists of steep topographic escarpments contained largely within Pleistocene glacial outwash sediments (Booth, 1989; Drury, 2001; Benda and Collins, 1992) and debris flow and earth flow deposits at the base. Glacial outwash sediments range broadly in character, from laterally continuous homogenous clay-rich sediments to lenticular, discontinuous packages of well-rounded and lithologically heterogeneous gravel. Together, the steep local relief and fine-grained strata of the Gold Basin landslide contribute to its large sediment delivery to the South Fork Stillaguamish River (Benda and Collins, 1992; Drury, 2001).

Several previous investigations focused on slope stability of the Gold Basin landslide and nearby landslide complexes and have estimated the mechanisms and volumes of sediment delivered from the Gold Basin landslide into the South Fork Stillaguamish River. Miller (1999) found that the lateral and vertical heterogeneity of Pleistocene glacial outwash strata leads to high groundwater flow in localized areas. Specifically, this is thought to occur when permeable sand and gravel is deposited over relatively impermeable clay and silt (Miller, 1999). McCabe (2016) measured stratigraphic columns within the middle lobe of the Gold Basin landslide and observed that sand and gravel deposited over fine impermeable layers did indeed correlate to perched ground water flow. The stratigraphy and groundwater observations suggest that erosion within the Gold Basin landslide may be concentrated along the upper extent of the exposed headwalls (McCabe, 2016). In addition to the concentration of groundwater flow, the shrinking and swelling of clay and silt-rich layers during wet and dry seasons leads to vertical cracking and block failure within the Gold Basin landslide (Shannon & Wilson Engineers, 1954).

The sediment and slope characteristics of the Gold Basin landslide lead to an overall large contribution of sediment delivery to the South Fork Stillaguamish River, estimated to be 25 percent of the total annual sediment load (40,000 tons per year from the Gold Basin landslide) (Benda and Collins, 1992). In a more quantitative effort, McCabe (2016) used terrestrial lidar scanning (TLS) and measured a net volumetric loss of 4,800 m^3 of the middle lobe of the Gold Basin landslide over a 6-month investigation (July to January). With the given density of dry glacial outwash (2,160 kg/m^3, Savage and others, 2000), this amounts to an annual contribution of about 11,500 tons from the middle lobe alone.
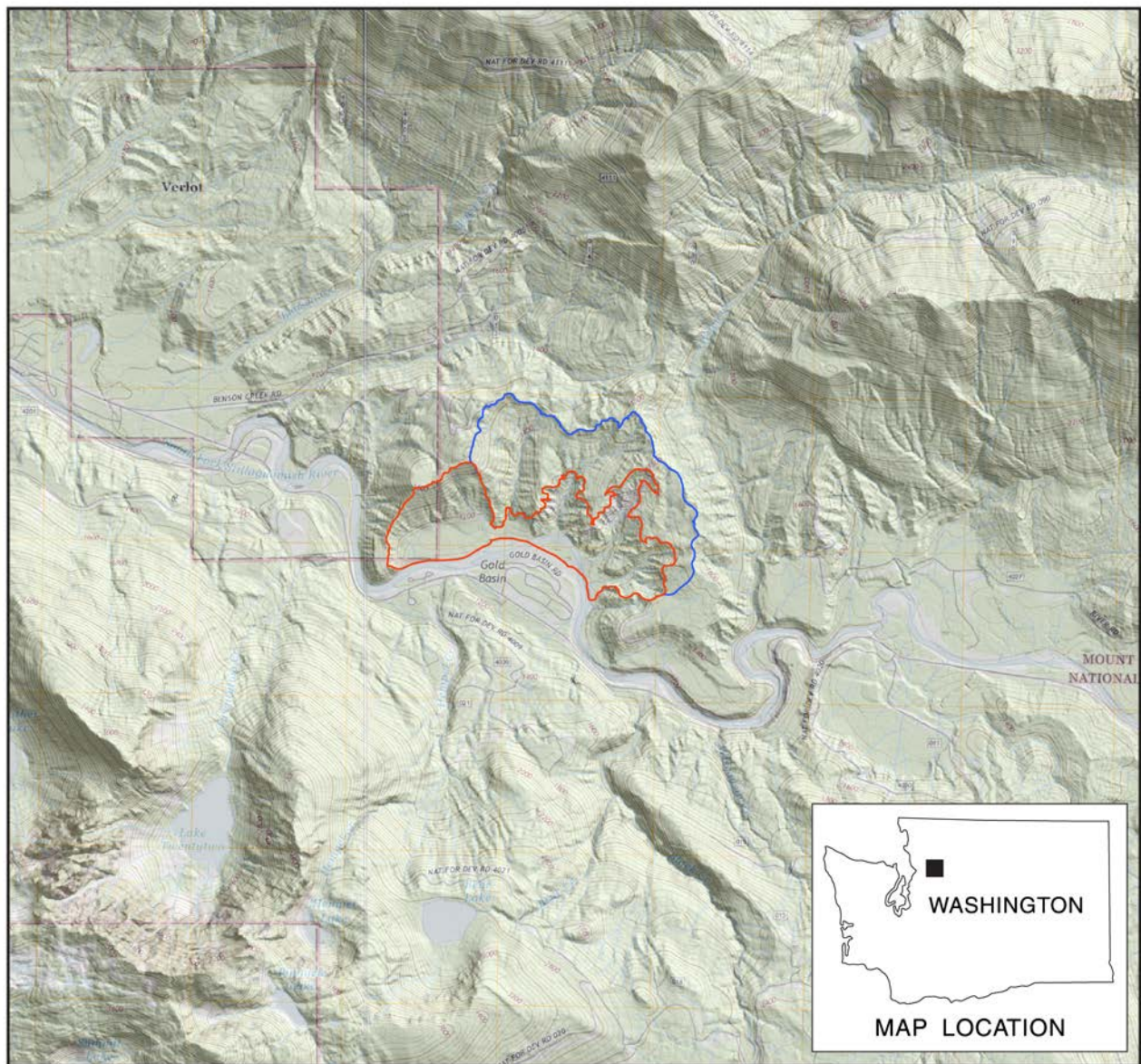
Figure 1. Topographic map of Gold Basin, Washington (2017 Whitehorse Mountain, 2017 Helena Ridge, 2017 Silverton, and 2017 Mallardy Ridge quadrangles), overlain by lidar hillshade map from the 2005 Snohomish and 2013 Tulalip lidar surveys (http://lidarportal.dnr.wa.gov/) of the Gold Basin landslide area. Inset map shows location of Gold Basin in Washington State. Red outline shows the three main lobes of the Gold Basin landslide. Blue outline shows area of mass wasting that is less well defined than the three lobes.

Assuming the three lobes equally supply sediment to the South Fork Stillaguamish River and that the Gold Basin landslide sediment contribution is similar over the other six months of the year, the TLS results may suggest an overall annual sediment delivery over 34,000 tons, only slightly less than suggested by Benda and Collins (1992). The main mechanisms of sediment delivery to the South Fork Stillaguamish River are from debris flows and erosion of exposed headwalls and prior landslide deposits (Benda and Collins, 1992; Miller, 1999).

In addition to landslides confined within the Pleistocene glacial strata, bedrock landslides are also apparent on lidar imagery of the study area (fig. 2). Bedrock landslides may pose additional hazard to the area, either during stochastic hillslope failure or during strong ground motion events (Meunier and others, 2007, 2008). Potential seismic sources include the proximal Darrington-Devils Mountain and southern Whidbey Island fault zones, as well as the offshore Cascadia Subduction Zone (Atwater and Hemphill-Haley, 1997; Witter and others, 2003; Sherrod and others, 2008; Personius and others, 2014). Previous analyses of hillslope stability in the Cascade Range suggests that rock mass strength (RMS) is a useful way of characterizing bedrock and fracture patterns in order to understand potential landslide-prone landscape (Schmidt and Montgomery, 1996).

Scope of Investigation

The goals of this investigation are to assess the glacial strata and bedrock geology of the Gold Basin landslide and adjacent areas and to assess how the geology and geomorphology within the study area affect the likelihood of coseismic landsliding.

Bedrock Mapping

Bedrock mapping initiated with the review of existing geologic maps and the current state of knowledge on rock units within the project area, followed by field work and the assessment of potential geologic influence on slope stability. Methods required field verification of rock units underlying the landslide to determine how glacial stratigraphy and bedrock geology can affect the likelihood of coseismic landslides, and to use quasi-quantitative RMS measurements to assess slope stability in various geologic units.

Seismic Hazard Assessment

Seismic hazard assessment initiated with a review the known seismicity in the area and to assess nearby structural features that could affect landslide behavior in the Gold Basin landslide vicinity during seismic events. This was followed by an estimation of maximum credible ground acceleration and discussion of expected duration of inter-event intervals for seismic events.

Bedrock Mapping

Methods

Fieldwork was conducted during the week of August 7, 2017. The focus of fieldwork was to assess Pleistocene glacial outwash sediment stratigraphy and slope stability and to assess bedrock strength near and within the Gold Basin landslide complex.

Pleistocene glacial outwash field sites were located within the Gold Basin landslide and along the eroded cut banks of the South Fork Stillaguamish River. Several key observations were noted at each site: (1) local stratigraphy, including bedding thickness and composition, (2) ground water flow out of the glacial outwash sediments, (3) fracture density and orientation with respect to hillslope, (4) maximum cliff height, and (5) evidence of recent hillslope failure.

PRELIMINARY GEOLOGIC MAP OF THE SOUTH FORK OF THE
STILLAGUAMISH RIVER; GOLD BASIN LANDSLIDE

Shaded relief image from
Snohomish 2005 lidar,
Tulalip 2013 lidar, and USGS
1/3-arc-second National
Elevation Dataset (NED).

Lambert Conformal Conic projection,
Central meridian 122° W
North American Datum 1927

SCALE 1:100 000

Geology compiled 2012–2017

WASHINGTON

MAP LOCATION

LIST OF MAP UNITS

Ice

Water

Qa — Quaternary alluvium

Qta — Quaternary talus deposits

Qp — Quaternary peat deposits

Qls
- Quaternary mass-wasting primary deposits, mostly landslides
- Quaternary mass-wasting primary headscarp, mostly landslides
- Quaternary mass-wasting secondary deposits, mostly landslides
- Quaternary mass-wasting secondary headscarp, mostly landslides

Qad — Pleistocene alpine glacial drift, Fraser-age

Qga — Pleistocene advance continental glacial outwash, Fraser-age, Vashon Stage

Qga(tb) — Pleistocene advance continental glacial outwash, Fraser-age, transitional beds

Qgo — Pleistocene continental glacial outwash, Fraser-age

Qgpc — Pleistocene continental glacial drift and nonglacial deposits, pre-Fraser, Vashon Stage

Qgt — Pleistocene continental glacial till, Fraser-age, Vashon Stage

Ɍec — Eocene continental sedimentary rocks

KJmm(w) — Cretaceous–Jurassic marine metasedimentary rocks of the western mélange belt

KJmv(w) — Cretaceous–Jurassic metavolcanic rocks of the western mélange belt

KJph(w) — Cretaceous–Jurassic low-grade phyllite of the western mélange belt

JȾmc(e) — Jurassic–Triassic cherty metasedimentary rocks of the eastern mélange belt

JȾmt(e) — Jurassic–Triassic metasedimentary and metavolcanics rocks of the eastern mélange belt

JMmt(t) — Jurassic–Mississippian metasedimentary and meta-volcanic rocks of the Trafton terrane

Ɍit(s) — Oligocene tonalite of Squire Creek stock

Ɍig(p) — Eocene rhyolite flows of Hansen Lake

Ɍvr(h) — Eocene granite of Mount Pilchuck stock

pTigd(b) — pre-Tertiary granodiorite of Mount Bald pluton

pTigd(bs) — pre-Tertiary granodiorite of Mount Bald pluton, sills

Jigb(e) — Jurassic gabbro of the eastern mélange belt

Jigbd(w) — Jurassic gabbro and diorite of the western mélange belt

Jit(e) — Jurassic tonalite of the eastern mélange belt

Ju(e) — Jurassic ultrabasic rocks of the eastern mélange belt

Ju(w) — Jurassic ultrabasic rocks of the western mélange belt

Mzu(h) — Mesozoic ultrabasic rocks of the Helena Haystack mélange

EXPLANATION OF MAP SYMBOLS

Contact

Normal fault—Solid where location is accurate, dashed where location is approximate, dotted where location is inferred

Thrust fault—Solid where location is accurate, dashed where location is approximate, dotted where location is concealed

Anticline—Solid where location is accurate, dotted where location is concealed

Bedding—Showing approximate strike and direction of dip

Vertical bedding—Showing strike

Inclined crinkled or deformed metamorphic or tectonic foliation—Showing approximate strike and dip

Vertical or near-vertical crinkled or deformed metamorphic or tectonic foliation—Showing approximate strike

Lidar boundary

Field Stations
- ○ Qls/Qgo
- ○ KJph(w)
- ○ JȾmt(e)

Figure 2. Preliminary geologic map of the South Fork Stillaguamish river centered over the Gold Basin landslide, Washington. Basemap is a lidar hillshade image derived from the Snohomish 2005 and Tulalip 2013 lidar datasets (http://lidarportal.dnr.wa.gov/) and the U.S. Geological Survey National Elevation Dataset (NED). Original mapping is from Pessl and others (1989) and Tabor and others (1988, 2002). New field sites are denoted by colored dots and site locations and descriptions are available in table 2).

Bedrock field sites were located within the South Fork Stillaguamish watershed within a 15 km radius of the Gold Basin landslide. To assess the potential for deep-seated landslides in bedrock, hillslope strength was assessed using the RMS scheme from Selby (1980) and adapted by Schmidt and Montgomery (1996). Measurements include: (1) the strength of intact bedrock, assessed using Schmidt hammer measurement; (2) the degree of bedrock weathering; (3) the orientation of discontinuities with respect to hillslope, including bedding, foliation, and cleavage; (4) the width of observed discontinuities; (5) the lateral and vertical pervasiveness and degree of clay infilling of discontinuities; and (6) the

5

movement of groundwater out of the rock mass (table 1). Observations were made during the dry season of 2017, which was a particularly dry year in western Washington, and therefore groundwater flow was observed at near-minimum flow levels.

Following fieldwork, bedrock mapping was entered and digitized in Esri ArcGIS, guided by existing 1:100,000 scale mapping (Pessl and others, 1989; Tabor and others, 1988, 2002). Landslides were mapped remotely using available lidar imagery and the landslide mapping protocol from Burns and Madin (2009). Aside from landslide mapping, geologic contacts were only changed from the original mapping where field observations or lidar imagery clearly showed need for amendment. The resulting geologic map is to be considered preliminary (fig. 2).

Table 1. Rock Mass Strength (RMS) parameters and relative rating (R)

Parameter	Very strong	Strong	Moderate	Weak	Very weak
Intact rock strength	Very coherent R=20	Coherent R=18	Moderate coherent R=14	Weak R=10	Very weak R=5
Weathering	Unweathered R=10	Slightly weathered R=9	Moderately weathered R=7	Highly weathered R=5	Completely weathered R=3
Discontinuity Spacing	>3 m R=30	3–1 m R=28	1–0.3 m R=21	0.3–0.05 m R=15	<0.05 m R=8
Discontinuity orientation with respect to hillslope	Moderate dip into slope R=20	Steep dip into slope R=18	Horizontal or vertical dip R=14	Steep dip out of slope R=9	Moderate dip out of slope R=5
Discontinuity width	<0.1 mm R=7	0.1–1 mm R=6	1–5 mm R=5	5–20 mm R=4	>20 mm R=2
Discontinuity pervasiveness and infilling	None pervasive R=7	Few pervasive R=6	Pervasive, no infill R=5	Pervasive, thin infill R=4	Pervasive, thick infill R=1
Outflow of ground water	None R=6	Trace R=5	<25 liters per m/102 R=4	25–125 liters per m/102 R=3	>125 liters per m/102 R=1
Total	**100–91**	**90–71**	**70–51**	**50–26**	**<26**

Field Observations

Thirty-one field sites were visited within the Gold Basin landslide area. Table 2 includes a list of field site locations and measurements taken. Field site locations are also shown on figure 2 and color-coded based on geologic unit. An expanded list of pertinent field observations is included below:

Site 2–1. Steep exposure of glacial outwash. Strata are mostly sandy with some pebble-rich layers. Horizontal bedding. Cliffs are ~13 m high.

Site 2–2. Steep exposure of glacial outwash. More conglomeratic layers than site 2–1.

Site 2–3. Steep 21.4-m-high cliff of glacial outwash. Base is conglomerate with pebble- to cobble-sized clasts. Strata fine upward into sand.

Site 2–4. Outcrop at this site is higher in glacial outwash stratigraphy. Units are sandier and seem more indurated. Vertical joints are more closely spaced. Horizontal bedding is more closely spaced.

Site 2–5. Cliff exposure consists of 130-m of glacial outwash. Hummocky wet clay landslide and debris flow deposits at base of cliffs. Debris flows at base of escarpment are very water laden. Stratigraphy at base of cliffs is thick and sandy with interbedded cobble-rich lenses. Generally fines upward. Beds are finely laminated near top. Cliffs fail as flakes along vertically oriented joint planes. Joint spacing appears to decreases in finer units towards top of cliffs.

Site 2–6. Small landslide in glacial outwash. Deposit is mainly composed of sand and pebble sized gravel.

Site 3–2. Glacial outwash exposure along South Fork Stillaguamish River. 16.8-m-high exposure. Base is pebble-cobble conglomerate fining upwards into sand. Upper layers are finely laminated 205-cm-thick beds. Crest of cliff is boulder conglomerate with scour at base. Energetic channel fill layer mimics topography.

Site 3-7. Glacial outwash exposure along Mountain Loop Highway. Base of outcrop is pebble conglomerate that fines to medium-coarse sand. Top is cobble conglomerate with both very well rounded and angular clasts.

Site 4–1. Glacial outwash exposure along South Fork Stillaguamish River. Fine-medium sand holds overhanging cliff angle. Swaley cross-bedding, up to 1-m-thick beds. Block failure calves off along vertically oriented fractures. Blocks are 1–10 cm thick.

Site 4–2. Glacial outwash exposure along South Fork Stillaguamish River. Very clay-rich unit at river level, extended upwards several meters. Top of clay-rich exposure is not clear at outcrop. Several interbedded gravel layers are present, non-cliff-forming exposure.

Site 4–3. Underlying competent bedrock exposure [KJph(w)] at crest of ridge. Glacial outwash likely a thin veneer at this site.

Site 4–4. Glacial outwash exposure along South Fork Stillaguamish River. Cliff is 41.8 m high. Cobble-rich layers do not hold cliff angle as well as sandy layers. Sandy units may have fine cementation, perhaps glacial rock flour or clay. Water trickling out of base of cobble-rich layers with finer strata beneath. Cobble-rich layers act as local aquifer. Observed water flow out of cliff up to 30.2 m above river level.

Site 4–5. Small outcrop of glacial outwash along South Fork Stillaguamish River. Gray clay-rich unit with interbedded cobble-rich layers. Unclear at outcrop whether cobble layers are interbedded or if they are more recent channel fill.

Site 4–6. Glacial outwash exposure capped by Quaternary alluvium. Glacial outwash exposure extends 2.4 m above river level. From 2.4–8.0 m, alluvium. Glacial outwash is fine and flakey clay-rich strata with few to no interbedded pebble clasts.

Site 4–7. Glacial outwash exposure along Marten Creek. Cliff exposure is 16.8 m high. Strata is very clay rich and dark gray in color. Glacial strata are capped with 4.4 m of Quaternary alluvium (cobble size fraction). Glacial clay strata are water laden.

Site 4–11. Near top of local glacial outwash elevation exposure limit. Top 7.8 m exposed is light gray in color and sandy. Locally more well indurated than most previous outcrops. Fractures are vertically oriented. Below sandy unit, 2 m of strata that are similarly gray but more clay rich than overlying sands. Induration is less well developed. Cobble conglomerate with sandy matrix 5.8 m below last exposure. Hillslope here and below is much more easily eroded. Finer strata hold steeper hillslope angle.

Table 2. Field site locations, discontinuity orientations, Schmidt hammer measurements, and RMS values

[Latitude and longitude in decimal degrees north and west. RMS, rock mass strength; no., number]

Site	Latitude	Longitude	Unit	Foliation		Joint set 1		Joint set 2		Joint set 3		Schmidt Hammer		RMS
				Strike	Dip	Strike	Dip	Strike	Dip	Strike	Dip	Average	No.	
1–1	48.07003	121.71677	KJph(w)	333	62	245	66	-	-	-	-	35.5	11	62
2–1	48.08147	121.73220	Qgo	-	-	-	-	-	-	-	-	-	-	49
2–2	48.08044	121.73182	Qgo	-	-	-	-	-	-	-	-	-	-	50
2–3	48.08033	121.72911	Qgo	-	-	-	-	-	-	-	-	-	-	58
2–4	48.08120	121.72797	Qgo	-	-	-	-	-	-	-	-	-	-	48
2–5	48.08205	121.72724	Qgo	-	-	-	-	-	-	-	-	-	-	-
2–6	48.07364	121.66096	Qgo	-	-	-	-	-	-	-	-	-	-	-
2–7	48.07259	121.65417	JŦrmt(e)	310	48	-	-	-	-	-	-	24.7	12	65
2–8	48.06582	121.70238	KJph(w)	338	9	195	83	292	89	-	-	42.8	10	77
2–9	48.06465	121.70314	KJph(w)	18	22	269	83	110	77	-	-	59.2	13	70
3–1	48.09281	121.74638	Qgo	-	-	-	-	-	-	-	-	-	-	-
3–2	48.08536	121.76214	Qgo	-	-	-	-	-	-	-	-	-	-	55
3–3	48.07760	121.74988	KJph(w)	348	17	205	37	296	44	-	-	32.2	11	64
3–4	48.03886	121.68658	KJmm(w)	236	16	64	71	17	78	117	79	46.4	15	77
3–5	48.03689	121.69669	KJmm(w)	-	-	-	-	-	-	-	-	43.4	15	-
3–6	48.02554	121.68753	KJmm(w)	356	88	70	76	28	25	-	-	59.1	12	85
3–7	48.04906	121.62963	Qgo	-	-	-	-	-	-	-	-	-	-	-
3–8	48.04907	121.63261	KJph(w)	124	57	-	-	-	-	-	-	23.7	17	62
3–9	48.04667	121.64910	KJph(w)	189	19	305	87	106	49	-	-	56.5	11	77
3–10	48.05255	121.66433	KJph(w)	84	58	278	85	-	-	-	-	44.6	7	62
4–1	48.07055	121.72056	Qgo	-	-	-	-	-	-	-	-	-	-	52
4–2	48.07003	121.71804	Qgo	-	-	-	-	-	-	-	-	-	-	53
4–3	48.07005	121.71787	KJph(w)	-	-	-	-	-	-	-	-	-	-	-
4–4	48.07295	121.71619	Qgo	-	-	-	-	-	-	-	-	-	-	-
4–5	48.07242	121.66409	Qgo	-	-	-	-	-	-	-	-	-	-	-
4–6	48.07101	121.65158	Qgo	-	-	-	-	-	-	-	-	-	-	-
4–7	48.07199	121.60693	Qgo	-	-	-	-	-	-	-	-	-	-	-
4–8	48.07391	121.59732	JŦrmt(e)	166	85	251	65	-	-	-	-	55	14	67
4–9	48.10513	121.56806	Oit(s)	-	-	-	-	-	-	-	-	55.2	13	-
4–10	48.08428	121.77922	KJph(w)	224	57	319	73	29	34	-	-	54.5	10	69
4–11	48.08346	121.77143	Qgo	-	-	-	-	-	-	-	-	-	-	-

Rock Mass Strength Results

Hillslope strength is set by several characteristics of bedrock, including intact rock strength and discontinuity spacing, width of separation along the joint, pervasiveness, and orientation with respect to hillslope (Schmidt and Montgomery, 1996). The RMS scheme outlined in table 1 (Selby, 1980; Schmidt and Montgomery, 1996) was used to assess RMS values. Each parameter listed bears on hillslope stability, however, Schmidt and Montgomery (1996) found that intact rock strength and discontinuity orientation with respect to hillslope are particularly key parameters. For instance, hillslopes with anaclinal discontinuity orientations, where discontinuities dip into the hillslope, are more stable than cataclinal orientations, where discontinuities dip out of the hillslope (Schmidt and Montgomery, 1996).

Intact rock strength was measured using a Schmidt hammer, which measures the recoil distance of a small piston hammer. Multiple Schmidt hammer measurements were taken at each bedrock site. Measurements were discarded if they were erroneously measured on flakes or otherwise non-intact rock at each outcrop (thus the exclusion of measurements in glacial outwash sediments). Bedrock field sites were located within one of three units: KJph(w), Jurassic to Cretaceous low-grade phyllite of the western mélange belt; KJmm(w), Jurassic to Cretaceous marine metasedimentary rocks of the western mélange belt; and JTrmt(e), Triassic to Jurassic metasedimentary and metavolcanic rocks of the eastern mélange belt. A summary of Schmidt hammer measurements is shown in figure 3.

Schmidt hammer measurements taken from KJph(w) ranged from low, weak values (10–20) to competent values (60–70), indicating extremely variable rock strength within this particular phyllite unit (fig. 3*A*, *B*). Measurements taken from KJmm(w) were less variable, and ranged typically between 30 and 65 (fig. 3*A*, *C*), showing overall greater rock competence than KJph(w). Discontinuity spacing was generally smaller and more pervasive in KJph(w), decreasing its overall RMS score. Finally, Schmidt hammer measurements taken on JTrmt(e) varied widely but were also strongly bimodal, with one population between about 20 and 31 and another population between 48 and 65 (fig. 3*A*, *D*). This suggests that rock competence may be generally quite strong for JTrmt(e), but local weathering or bedrock characteristics can weaken the local strength of the unit and, therefore, decrease hillslope stability.

To assess discontinuity orientation with respect to hillslope, foliation and joint-set orientations were measured using a Brunton compass (table 2). In general, the strongest joint-set pattern trends northwest-southeast for measured sites and for previously mapped foliations (fig. 2; table 2). Jurassic to Cretaceous units (KJmm(w) and KJph(w)) often had 2–3 prominent joint-set orientations, whereas the Triassic to Jurassic units (JTrmt(e)) had fewer prominent joint-set patterns. However, few sites were visited and these observations may not be characteristic of the entire study area.

Hillslope aspect and slope was measured at each site from existing digital elevation models and compared to discontinuity orientations (table 3). Table 3 reports the absolute difference of hillslope versus discontinuity strike orientation (Δ Strike) and the angular divergence (Δ Dip) between hillslope gradient and discontinuity dip. Low values of absolute orientation difference (Δ Strike <90°) are suggestive of cataclinal slopes. Low values of angular divergence (Δ Dip = 10°–40°) are particularly susceptible to deep-seated landsliding (Schmidt and Montgomery, 1996).

Overall, most bedrock sites were assigned "Moderate" RMS values (tables 1, 2). Sites that were assigned "Strong" RMS values were contained within either KJph(w) or KJmm(w) units (tables 1, 2). For a nearby study on existing slope failure and its correlation to RMS values, Schmidt and Montgomery (1996) found that landslide sites consistently had RMS values below 69. Fifty percent of RMS values at bedrock sites are below 69 (table 3). Several RMS values were assessed for glacial outwash sites where "intact rock strength" is essentially at a minimum. These RMS values are consistently less than or equal to 50 and considered weak (tables 1, 2).
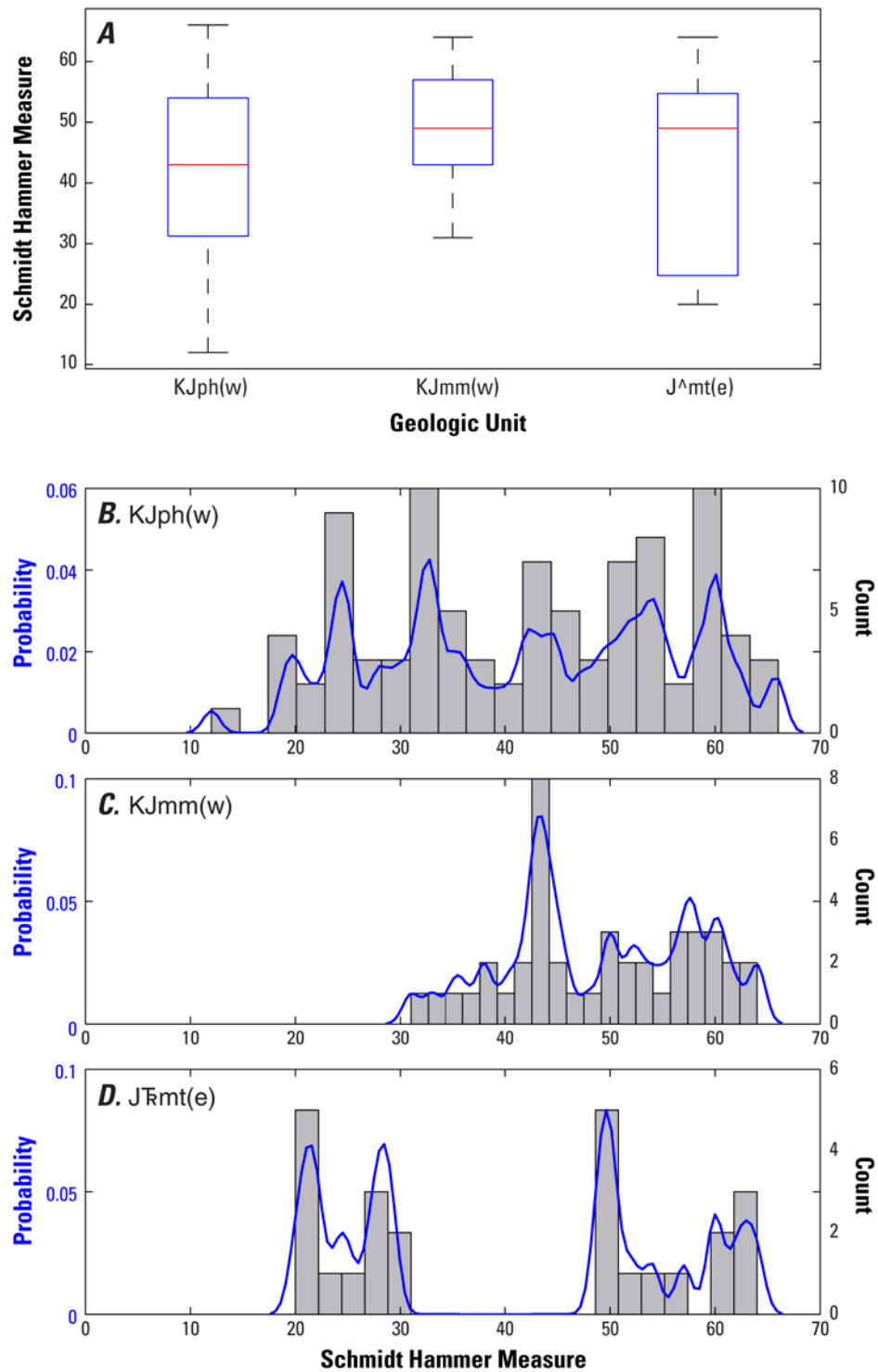
9

Figure 3. Statistical plots of Schmidt hammer measurements from bedrock sites within the Gold Basin landslide study area, Washington. *A*, Box and whisker plots showing the mean value (red line) and range (black bracketed lines) of Schmidt hammer measurements for three different geologic units. *B–D*, Probability density functions (blue lines) and histograms (gray boxes) of individual Schmidt hammer measurements of KJph(w) (*B*), KJmm(w) (*C*), and JŦmt(e) (*D*).

10

Table 3. Discontinuity orientations with respect to hillslope and Rock Mass Strength (RMS) parameters for bedrock field sites

[Bold values indicate low values of absolute orientation difference, angular divergence, or RMS values that may suggest slopes susceptibility to deep-seated landsliding. WRT, with respect to; RMS, rock mass strength; no., number]

Site	Unit	Hillslope orientation		Foliation WRT slope		Joint set 1 WRT slope		Joint set 2 WRT slope		Joint set 3 WRT slope		Schmidt Hammer		RMS	
		Strike	Dip	Δ Strike	Δ Dip	Δ Strike	Δ Dip	Δ Strike	Δ Dip	Δ Strike	Δ Dip	Average	No.		
2–7	JR̄mt(e)	136.3	6.9	173.7	41.1	-	-	-	-	-	-	24.7	12	**65**	Moderate
4–8	JR̄mt(e)	80.0	15.5	86.0	69.5	171.0	49.5	-	-	-	-	55.0	14	**67**	Moderate
3–4	KJmm(w)	289.1	3.6	**53.1**	**12.4**	225.1	67.4	272.1	74.4	172.1	75.4	46.4	15	77	Strong
3–6	KJmm(w)	182.9	0.2	173.1	87.8	112.9	75.8	154.9	24.8	-	-	59.1	12	85	Strong
1–1	KJph(w)	78.9	2.9	254.1	59.1	166.1	63.1	-	-	-	-	35.5	11	**62**	Moderate
2–8	KJph(w)	236.0	6.2	102.0	2.8	41.0	76.8	56.0	82.8	-	-	42.8	10	77	Strong
2–9	KJph(w)	296.8	6.0	278.8	16.0	27.8	77.0	186.8	71.0	-	-	59.2	13	70	Moderate
3–3	KJph(w)	290.6	5.2	**57.4**	**11.8**	85.6	31.8	**5.4**	**38.8**	-	-	32.2	11	**64**	Moderate
3–8	KJph(w)	322.9	4.0	198.9	53.0	-	-	-	-	-	-	23.7	17	**62**	Moderate
3–9	KJph(w)	235.0	4.0	**46.0**	**15.0**	70.0	83.0	129.0	45.0	-	-	56.5	11	77	Strong
3–10	KJph(w)	304.9	7.5	220.9	50.5	26.9	77.5	-	-	-	-	44.6	7	**62**	Moderate
4–10	KJph(w)	296.9	3.1	72.9	53.9	22.1	69.9	267.9	30.9	-	-	54.5	10	69	Moderate

To obtain a larger-scale view of bedrock controls on slope stability, I analyzed the number of mapped landslides that originate in various lithologic units (fig. 4) and how slope values vary with lithologic unit. The results show that Pleistocene glacial strata have a greater number of landslides contained within the units relative to other bedrock units, followed by Jurassic to Cretaceous metamorphosed mélange units (KJmm(w) and KJph(w)). The relatively large number of landslides mapped within Pleistocene glacial strata may be due to the unconsolidated nature of these units. Jurassic to Cretaceous mélange may also be more susceptible to landsliding than other units owing to the greater number of prominent joint sets observed, which may contribute to degraded slope stability if cataclinally oriented with hillslope. Slope values analyzed for various geologic units are generally inversely correlated with landslide abundance, which may suggest that the relatively unconsolidated strata and highly fractured bedrock units are less likely to maintain steep hillslope angles. While Jurassic to Cretaceous and Pleistocene units also compose a large proportion of the area, the number of landslides does not entirely correlate to the percentage of analyzed area composed of each lithology (fig. 4).
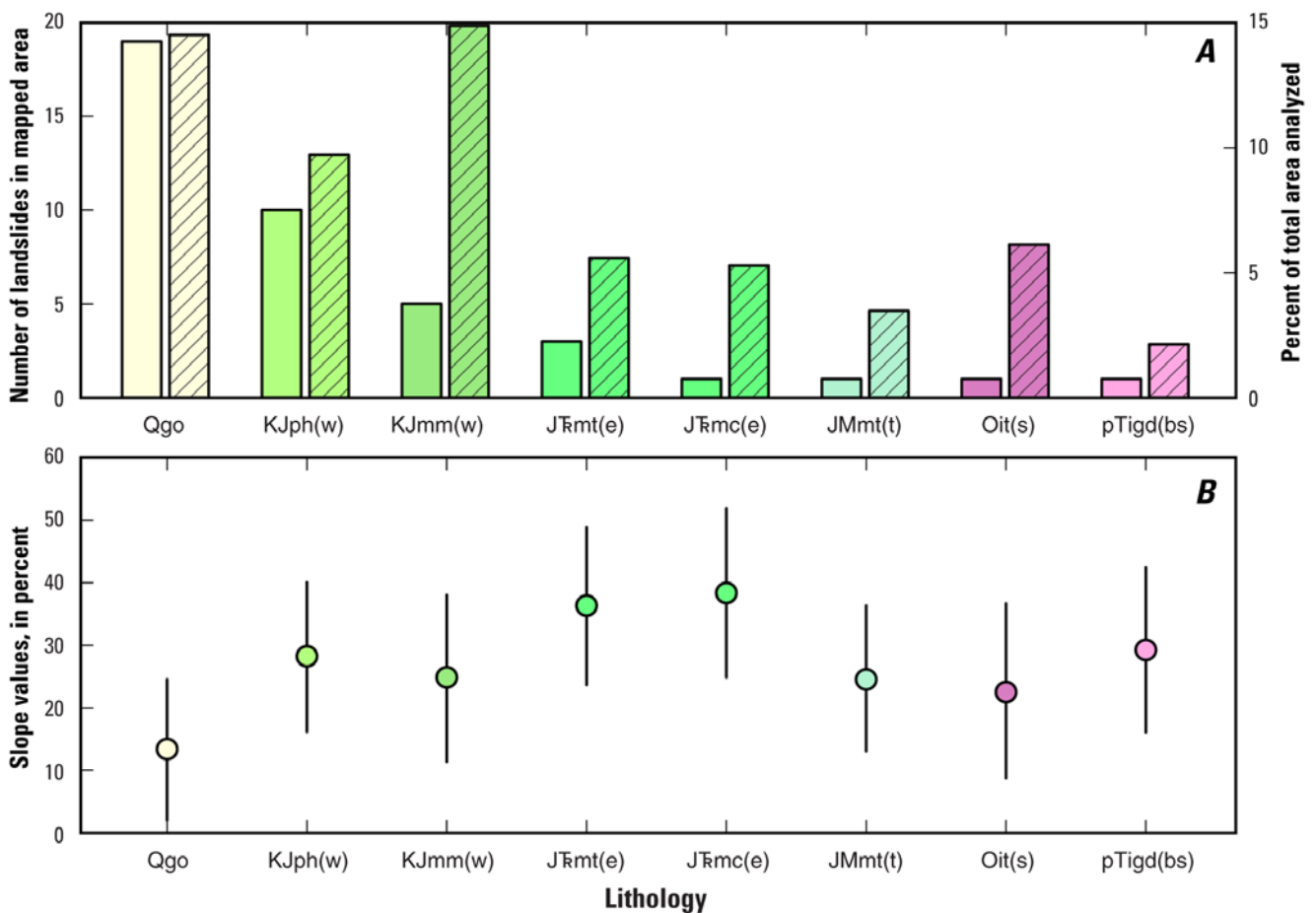
Figure 4.   Plots of landslides and slope values by geologic unit in the Gold Basin landslide study area (see fig. 2 for locations of units). *A*, The number of landslides with significant area and (or) headscarps originating in each geologic unit and the percentage of land composed of each lithology (hatched bars). *B*, The mean and standard deviation of slope values analyzed for each geologic unit. The number of landslides and slope angles are broadly inversely correlated.

Seismic Hazard Assessment

Seismic hazards in western Washington State come from two main sources: megathrust earthquakes along the Cascadia Subduction Zone (Peterson and others, 2008), located offshore to the west, and smaller but shallower earthquakes along upper crustal faults in the Puget Sound lowland (Sherrod, 2001; Sherrod and others, 2000, 2004; Nelson and others, 2003a,b; Sherrod and Gomberg; 2014; Personius and others, 2014). Consequently, a recent Probabilistic Seismic Hazard Assessment (PSHA) of the United States shows seismic hazard potential in western Washington is relatively high (fig. 5) (Peterson and others, 2008). The magnitude of ground shaking correlates well with the volume and aerial extent of coseismic landsliding (Keefer, 1994, 2002; Meunier 2007, 2008) owing to the addition of short-lived stresses that can exceed the cohesion and frictional strength of hillslopes (Newmark, 1965). Thus, estimates of the probability of peak ground acceleration (PGA) magnitude and frequency are useful for identifying and characterizing landslide hazards.
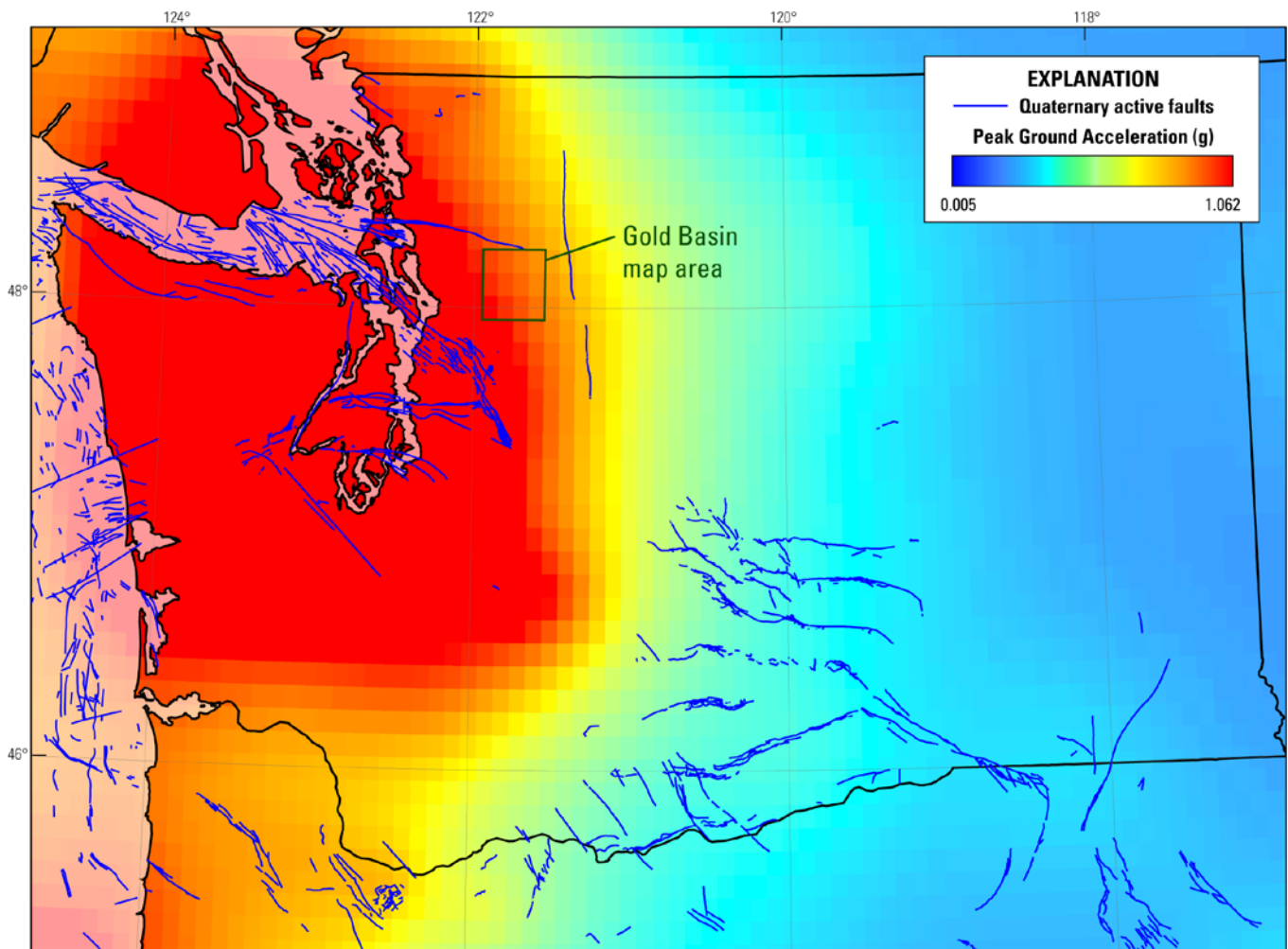
Figure 5. Probabilistic Seismic Hazard map of Washington State (from Peterson and others, 2008). Cool to warm color gradient shows the peak ground acceleration (PGA) values with a 10 percent probability of expected exceedance within the next 50 years. Quaternary active faults are from the U.S. Geological Survey Quaternary fault and fold database (USGS, 2006).

For the Gold Basin landslide area, nearby active upper crustal faults include the Darrington-Devils Mountain fault zone to the north, which ruptured a $M6.7–M7.0$ earthquake about 2,000 years ago (Personius and others, 2014), and the southern Whidbey Island fault zone to the south, which generated four post-glacial surface rupturing earthquakes (Sherrod and others, 2008). Offshore, the Cascadia Subduction Zone is capable of producing great earthquakes ($M > 8$) (Atwater and Hemphill-Haley, 1997; Witter and others, 2003). Coseismic landsliding during the 1994 $M6.7$ Northridge and 1999 $M7.6$ Chi-Chi earthquakes has occured when PGA values exceed 1 meter per second squared (m/s^2), equivalent to 0.102 g (where g is the acceleration due to gravity), and on slopes that exceed 20° (Meunier and others, 2007, 2008). The Northridge and Chi-Chi earthquake locations are ideal for analysis because they represent case studies of coseismic landsliding in dry and wet conditions, respectively, at magnitudes expected from upper crustal faults in Washington. Therefore, critical PGA and slope values from Meunier and others (2007) were used in the following hazard analysis.

Probability of Ground Shaking Exceedance

In order to assess coseismic landslide hazard posed by onshore and offshore earthquake sources for the area proximal to the Gold Basin landslide, I extracted the 50-year seismic intensity hazard curve from the U.S. Geological Survey 2008 PSHA model (fig. 6) (Peterson and others, 2008). From the hazard curve, I extracted two horizontal dissections at 2 percent and 10 percent probability (fig. 6). The resulting probability density functions (PDFs) represent the 2 percent and 10 percent probability of ground shaking intensity to be exceeded over the next 50 years, respectively. These curves indicate that there is an estimated 2 percent probability of PGA greater than approximately 0.42 g in the study area in the next 50 years. There is an estimated 10 percent probability of PGA greater than approximately 0.215 g in the study area in the next 50 years. Both of these PGA values are greater than the critical PGA estimated from the Northridge and Chi-Chi earthquakes, above which coseismic landsliding occurred (Meunier and others, 2007).

Since the values at 2 percent and 10 percent probability of exceedance are above the critical PGA for coseismic landsliding (~0.102 g), I extracted a vertical dissection of the hazard curve at 0.1 g, which shows the distribution of exceedance probabilities for the specific value of shaking intensity (fig. 6). The resulting PDF shows that there is approximately a 37.5 percent probability of exceeding the 0.1 g ground shaking intensity in the next 50 years. From this, I infer that there is approximately a 37.5 percent probability coseismic landsliding will occur in the study area over the next 50 years on slopes greater than 20° (fig. 6).

Slope values in the study area are fairly steep on average (fig. 7). Of the lidar footprint analyzed (~1,047 km^2), over 530 km^2 of the area is steeper than 20°. Therefore, over half the total area shown in figure 7 is at a slope angle susceptible to coseismic landsliding if ground acceleration exceeds 1 m/s^2.

Bedrock Characteristics and Coseismic Hillslope Failure

The above seismic hazard assessment does not necessarily suggest that most or all hillslopes above 20° are likely to fail during a seismic event in the study area, but rather suggests that a considerable portion of the landscape in the area is available for failure. Local characteristics of the substrate, including rock type and orientation of discontinuities with respect to hillslope angle, are important as well. Based on fieldwork and analysis of bedrock characteristics, some bedrock sites appear to be more prone to slope failure, whether during a seismic event or not.
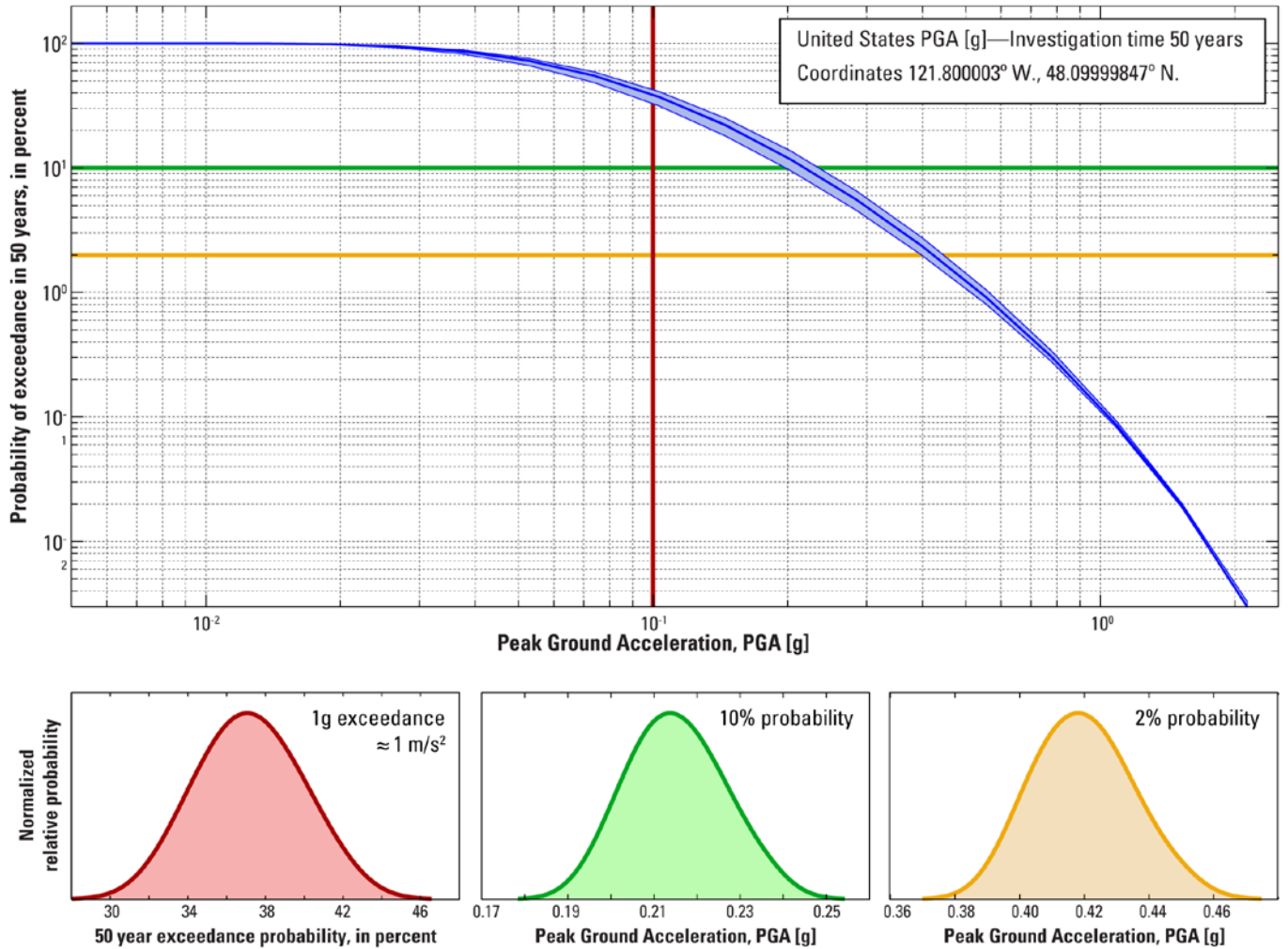
Figure 6. Probabilistic seismic hazard curve extracted from the U.S. Probabilistic Seismic Hazard Assessment map (Peterson and others, 2008) for the Gold Basin landslide study area, Washington. Values were extracted at lat. 48.1° N., long 121.8° W. Blue lines are the probabilistic curved generate for site-specific probability and peak ground acceleration (PGA) values. Red vertical line on the main plot is the distribution of exceedance probabilities for a specific value of ground **shaking intensity** (0.1 g ≈ 1 m/s^2 [where g is acceleration due to gravity]). Red curve below main plot shows the PDF of expected probabilities of exceedance for 0.1 g. Horizontal green and orange lines represent the PGA values extracted for specific probabilities (10 percent and 2 percent, respectively). These horizontal dissections are plotted as green and orange probability density functions (PDFs) below.
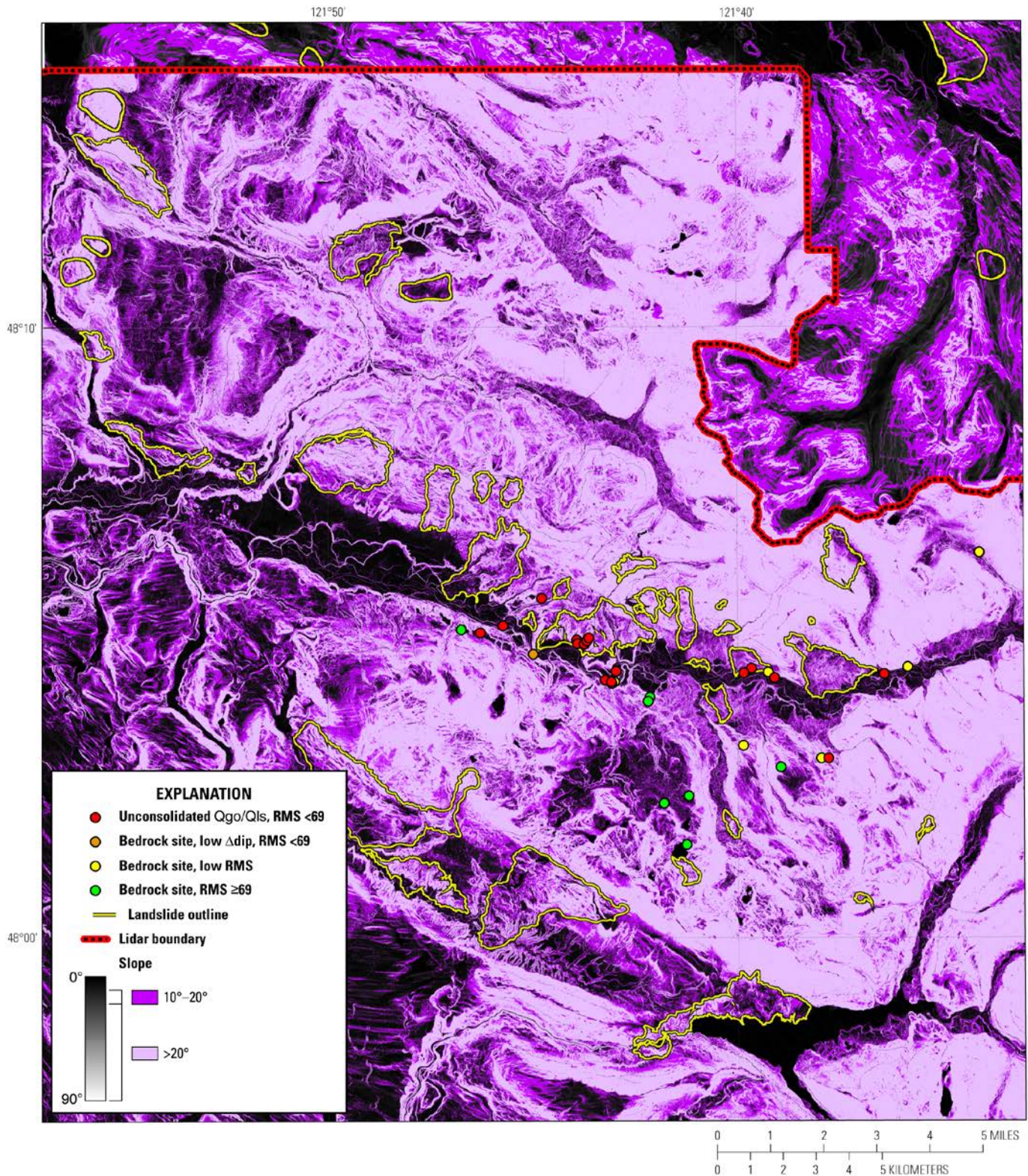
Figure 7. Slope map of the Gold Basin landslide study area, South Fork Stillaguamish River, Washington. Hillslopes between 10° and 20° are highlighted in darker purple. Hillslopes above 20° are highlighted in lavender. Bedrock, glacial outwash, and landslide field sites locations are shown with dots colored by potential landslide hazard. Red dots show sites in active landslides or unconsolidated glacial outwash strata, which indicates they are

16

active or have characteristics for potential shallow to deep-seated landslide; orange dots show bedrock sites with cataclinal discontinuity orientations, low dip divergence, and low rock mass strength (RMS) values, which indicates they have conditions for potential deep-seated hillslope failure; yellow dots show bedrock sites with low RMS values and anaclinal discontinuity orientations, which indicates they have some conditions characteristic of potential deep-seated hillslope failure; green dots show bedrock sites with high RMS values and anaclinal discontinuity orientations, which indicates they have few to no characteristics for potential hillslope failure.

The slope map in figure 7 also shows bedrock and landslide field sites color-coded by characteristics that may lead to slope failure. Sites that are either active landslides or are underlain by weak, unconsolidated Quaternary glacial strata are shown in red. Owing to the weak material properties, low RMS values, and already active landslides at these sites, the adjacent hillslopes appear to be relatively unstable. In addition, slope analyses suggest these strata do not typically maintain steep hillslope angles (fig. 4). Field sites in bedrock with low RMS values (RMS <69), low discontinuity dip divergence (10°–40°), and cataclinal discontinuity orientations are shown in orange. At these sites, vertically oriented topographic stresses will decrease the relative rock strength because joints and bedding layers (discontinuities) are optimally oriented to produce shear dislocation surfaces (Schmidt and Montgomery, 1996). Bedrock field sites with low RMS values and anaclinal discontinuity orientations are shown in yellow. While the intact rock strength and discontinuity characteristics suggest these sites are underlain by a relatively weak substrate, the anaclinal discontinuity orientations are such that vertically oriented topographic stresses increase relative rock strength. Finally, bedrock sites with relatively high RMS values and anaclinal discontinuity orientations are shown in green and are considered the most stable under passive conditions.

In the event of strong ground shaking, vertical and horizontal PGAs have the potential to push hillslopes closer to failure. This suggests that hillslopes with anaclinal discontinuity orientations are susceptible to coseismic landsliding if the dynamic seismically induced stresses sufficiently decrease cohesion or the internal angle of friction to allow for brittle failure (Newmark, 1965). Therefore, the characterization of field sites based on bedrock and hillslope measurements should be considered general and not indicative of absolute stability or instability.

References Cited

Anchor QEA, LLC, 2012, Final alternatives evaluation report Gold Basin landslide study: Seattle, Wash., Prepared for Stillaguamish Tribe of Indians, 167 p.

Atwater, B.F., and Hemphill-Haley, E., 1997, Recurrence intervals for great earthquakes of the past 3,500 years at northeastern Willapa Bay, Washington: U.S. Geological Survey Professional Paper 1576, 108 p.

Benda, L., and Collins, B., 1992, Slope Stability Investigation of the Crown Pacific Property in the South Fork of the Stillaguamish River Basin: unpublished report, 37 p.

Booth, D.B., 1989, Surficial geologic map of the Granite Falls 15-minute quadrangle, Snohomish County, Washington: U.S. Geological Survey Miscellaneous Investigations Series Map I-1852, scale 1:50,000, 3 sheets.

Burns, W.J., and Madin, I., 2009, Protocol for inventory mapping of landslide deposits from light detection and ranging (lidar) imagery: Portland, Oreg., Oregon Department of Geology and Mineral Industries, Special Paper 42, 30 p.

Drury, T., 2001, Gold Basin Landslide Remediation Feasibility Study, Alternatives development and analysis, and preliminary project designs, RM 48, SF Stillaguamish River: Prepared for the Stillaguamish Tribe of Indians, 45 p.

Keefer, D.K., 1994, The importance of earthquake-induced landslides to long-term slope erosion and slope-failure hazards in seismically active regions: Geomorphology, v. 10, no. 1–4, p. 265–284.

Keefer, D.K., 2002, Investigating landslides caused by earthquakes–a historical review: Surveys in Geophysics, v. 23, no. 6, p. 473–510.

McCabe, C., 2016, Using terrestrial lidar to monitor erosion within the Gold Basin landslide complex, Verlot, WA: Seattle, Wash., University of Washington, M.S. Thesis, 61 p.

Meunier, P., Hovius, N., and Haines, A.J., 2007, Regional patterns of earthquake-triggered landslides and their relation to ground motion: Geophysical Research Letters, v. 34, no. 20, 5 p.

Meunier, P., Hovius, N., and Haines, J.A., 2008, Topographic site effects and the location of earthquake induced landslides: Earth and Planetary Science Letters, v. 275, no. 3, p. 221–232.

Miller, D., 1999, Hazel/Gold Basin Landslides—Geomorphic Review Draft Report: M2 Environmental Services, 25 p.

Nelson, A.R., Johnson, S.Y., Kelsey, H.M., Sherrod, B.L., Wells, R.E., Okumura, K., Bradley, L.A., Bogar, R., and Personius, S.F., 2003a, Field and laboratory data from an earthquake history study of the Waterman Point fault, Kitsap County, Washington: U.S. Geological Survey Miscellaneous Field Studies Map MF-2423.

Nelson, A.R., Johnson, S.Y., Kelsey, H.M., Wells, R.E., Sherrod, B.L., Pezzopane, S.K., Bradley, L.A., Koehler III, R.D., and Bucknam, R.C., 2003b, Late Holocene earthquakes on the Toe Jam Hill fault, Seattle fault zone, Bainbridge Island, Washington: Geological Society of America Bulletin, v. 115, no. 11, p. 1388–1403.

Newmark, N.M., 1965, Effects of earthquakes on dams and embankments: Geotechnique, v. 15, no. 2, p. 139–160.

Personius, S.F., Briggs, R.W., Nelson, A.R., Schermer, E.R., Maharrey, J.Z., Sherrod, B.L., Spaulding, S.A., and Bradley, L.A., 2014, Holocene earthquakes and right-lateral slip on the left-lateral Darrington–Devils Mountain fault zone, northern Puget Sound, Washington: Geosphere, v. 10, no. 6, p. 1482–1500.

Pessl, F., Jr., Dethier, D.P., Booth, D.B., and Minard, J.P., 1989, Surficial geologic map of the Port Townsend 30-by 60-minute quadrangle, Puget Sound region, Washington: U.S. Geological Survey Miscellaneous Investigations Series Map I-1198–F.

Petersen, M.D., Frankel, A.D., Harmsen, S.C., Mueller, C.S., Haller, K.M., Wheeler, R.L., Wesson, R.L., Zeng, Y., Boyd, O.S., Perkins, D.M., Luco, N., Field, E.H., Wills, C.J., and Rukstales, K.S., 2008, Documentation for the 2008 Update of the United States National Seismic Hazard Maps: U.S. Geological Survey Open-File Report 2008–1128, 61 p.

Savage, W.Z., Morrissey, M.M., and Baum, R.L., 2000, Geotechnical properties for landslide-prone Seattle-area glacial deposits: U.S. Geological Survey Open-File Report 00–228, 6p.

Schmidt, K.M., and Montgomery, D.R., 1996, Rock mass strength assessment for bedrock landsliding: Environmental & Engineering Geoscience, v. 2, no. 3, p. 325–338.

Selby, M.J., 1980, A rock mass strength classification for geomorphic purposes, with tests from Antarctica and New Zealand: Zeitschrift fur Geomorphologie, v. 24, no.1, p. 31–51.

Shannon & Wilson Engineers, 1954, Report on slide on South Fork Stillaguamish River at Gold Basin Forest Camp: Prepared for the State of Washington Departments of Fisheries, 14 p., appendix, 9 plates.

Sherrod, B.L., 2001, Evidence for earthquake-induced subsidence about 1100 yr ago in coastal marshes of southern Puget Sound, Washington: Geological Society of America Bulletin, v. 113, no. 10, p. 1299–1311.

Sherrod, B.L., Blakely, R.J., Weaver, C.S., Kelsey, H.M., Barnett, E., Liberty, L., Meagher, K.L., Paper, K., 2008, Finding concealed active faults—Extending the southern Whidbey Island fault across the Puget lowland, Washington: Journal of Geophysical Research, v. 113, no. B5, 25 p.

Sherrod, B.L., Brocher, T.M., Weaver, C.S., Bucknam, R.C., Blakely, R.J., Kelsey, H.M., Nelson, A.R., and Haugerud, R., 2004, Holocene fault scarps near Tacoma, Washington, USA: Geology, v. 32 no. 1, p. 9–12.

Sherrod, B.L., Bucknam, R.C., and Leopold, E.B., 2000, Holocene relative sea level changes along the Seattle Fault at Restoration Point, Washington: Quaternary Research, v. 54, no. 3, p. 384–393.

Sherrod, B., and Gomberg, J., 2014, Crustal earthquake triggering by pre-historic great earthquakes on subduction zone thrusts: Journal of Geophysical Research, v. 119, no. B2, p. 1273–1294.

Tabor, R.W., Booth, D.B., Vance, J.A., and Ford, A.B., 1988, Geologic Map of the Sauk River 30-by 60-minute Quadrangle, Washington: U.S. Geological Survey Open-File Report 88–692.

Tabor, R.W., Booth, D.B., Vance, J.A., and Ford, A.B., 2002, Geologic map of the Sauk River 30- by 60-minute Quadrangle, Washington: U.S. Geological Survey Geologic Investigations Series Map I–2592, scale 1:100,000, 3 sheets.

Witter, R.C., Kelsey, H.M., and Hemphill-Haley, E., 2003, Great Cascadia earthquakes and tsunamis of the past 6700 years, Coquille River estuary, southern coastal Oregon: Geological Society of America Bulletin, v. 115, no. 10, p. 1289–1306